

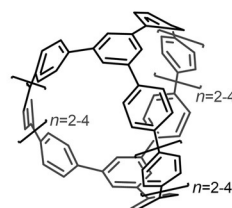
# Triple Helicene Cage: Three-Dimensional $\pi$ -Conjugated Chiral Cage with Six [5]Helicene Units

Tomoya Matsushima,<sup>[a]</sup> Shoko Kikkawa,<sup>[b]</sup> Isao Azumaya,<sup>[b]</sup> and Soichiro Watanabe\*<sup>[a]</sup>

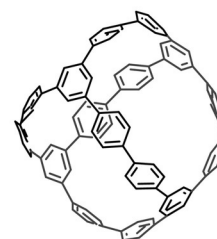
A three-dimensional  $\pi$ -conjugated chiral cage with six [5]helicene units (a triple helicene cage) was synthesized for the first time. Taking advantage of the Yamamoto coupling reaction, the triflate-substituted triple [5]helicene, a strained and preorganized precursor, was dimerized to afford the target compound. Single-crystal X-ray diffraction analysis revealed the unique structural features of the triple helicene cage: a cage-shaped rigid structure with outer helical grooves and an inner chiral cavity. All-*P* and all-*M* enantiomers were separated successfully by HPLC over a chiral column and their chiroptical properties were characterized by circular dichroism spectra.

Closed and three-dimensional (3D)  $\pi$ -conjugated hydrocarbons such as fullerenes and carbon nanotubes have received extensive attention in numerous research fields because of their aesthetic structures, unique properties, and various applications.<sup>[1]</sup> Development of the bottom-up strategy for the synthesis of 3D nanocarbons is a hot topic in organic chemistry and material sciences. In 2017, the carbon nanobelt, a milestone compound in this field, was reported.<sup>[2]</sup> However, construction of closed and 3D polycyclic aromatic hydrocarbons (PAHs) with fused ring systems remains a significant challenge. Cage-shaped conjugated hydrocarbons have been investigated over the last few decades as model compounds in nanoarchitecture studies<sup>[3a,b]</sup> or as precursors of fullerenes.<sup>[3c-g]</sup> Recently, cage-shaped phenylene multirings have been reported independently by the Itami<sup>[4]</sup> and Yamago<sup>[5]</sup> groups (Figures 1 A and 1B). These molecules consist exclusively of discrete benzene rings, in which *para*-phenylenes are linked by 1,3,5-tri-substituted benzene intersections. In these highly distorted compounds, the strain across the whole molecule was usually generated in the last step of their synthesis using relatively less strained pre-

Cage-shaped conjugated hydrocarbons

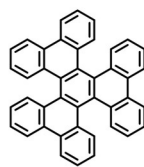


**A** (Itami, 2013, 2014)  
carbon nanocage



**B** (Yamago, 2013)  
ball-shaped phenylene multirings

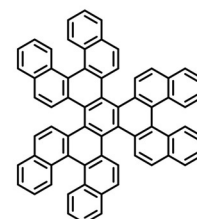
Threefold-symmetrical multiple helicenes



**HBTP**  
(Pascal Jr., 1999)  
triple [5]helicene



**T5H**  
(Watanabe, 2017)  
triple [5]helicene



**H5H**  
(Watanabe, Kamikawa, 2017)  
hexapole [5]helicene

**Figure 1.** Examples of cage-shaped  $\pi$ -conjugated hydrocarbons and threefold-symmetrical multiple helicenes.

cursors. Although these elegant methods have offered new strategies for the synthesis of *para*-phenylene-based multirings, they are not applicable to the construction of 3D highly strained fused-ring systems. Recently, we have reported threefold-symmetrical multiple helicenes, such as the triple [5]helicene **T5H**,<sup>[6]</sup> a structural isomer of hexabenzotriphenylene **HBTP**<sup>[7]</sup> and hexapole [5]helicene **H5H**<sup>[8]</sup> (Figure 1). These multiple helicenes have highly distorted structures, because of the repulsion of multiple [5]helicene units. In particular, the thermodynamically most stable isomer of **T5H**, synthesized through oxidative photocyclization,<sup>[9]</sup> can provide a unique platform with three functional groups at the tip of its peripheral moieties positioned on the same side of the molecule.

We considered that the structural features of **T5H** must represent a promising building unit to construct fused-ring 3D cage structures, because **T5H** is preorganized for the synthesis of cage molecules. **HBTP** and **H5H** are not always suitable building units for this particular purpose, because they suffer from possible formation of undesired isomers or conformations during their synthesis through the pyrolysis or cyclotrimerization of arynes. Herein, we report the synthesis and properties of a triple helicene cage (**THC 1**) that consists of 20 benzene rings with six [5]helicene units, and represents the first example of fused-ring  $\pi$ -conjugated 3D cage-shaped molecules.

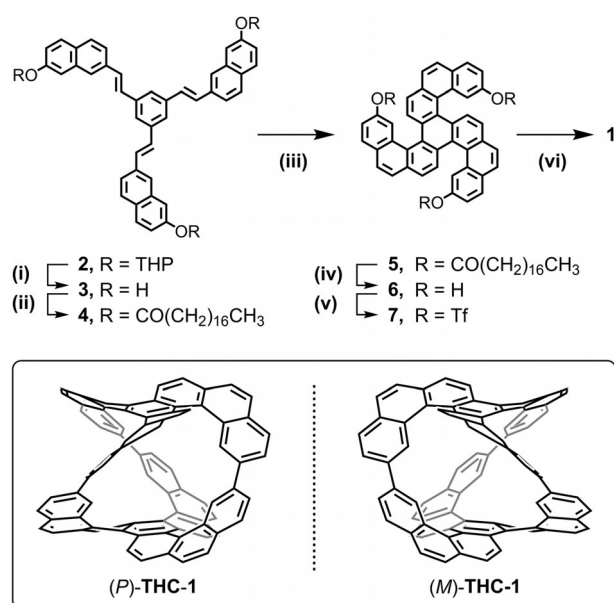
[a] T. Matsushima, Prof. Dr. S. Watanabe  
Department of Biomolecular Science  
Faculty of Science and Research Center for  
Materials with Integrated Properties, Toho University  
Miyama 2-2-1, Funabashi, Chiba 274-8510 (Japan)  
E-mail: soichiro@biomol.sci.toho-u.ac.jp

[b] S. Kikkawa, Prof. Dr. I. Azumaya  
Faculty of Pharmaceutical Sciences, Toho University  
Miyama 2-2-1, Funabashi, Chiba 274-8510 (Japan)

Supporting Information and the ORCID identification numbers for the authors of this article can be found under <https://doi.org/10.1002/open.201800006>.

© 2018 The Authors. Published by Wiley-VCH Verlag GmbH & Co. KGaA. This is an open access article under the terms of the Creative Commons Attribution-NonCommercial License, which permits use, distribution and reproduction in any medium, provided the original work is properly cited and is not used for commercial purposes.

Our strategy for the synthesis of **THC** includes oxidative photocyclization<sup>[10]</sup> for the construction of the **T5H** backbone and a subsequent aryl–aryl coupling reaction (Scheme 1). The yields of each step from compounds **2** to **7** were moderate to



**Scheme 1.** Synthesis of triple helicene cage **THC 1**. Reagents and conditions: i) 1 M HCl, 96%; ii) stearoyl chloride, TEA, 99%; iii)  $h\nu, I_2, \text{K}_2\text{CO}_3, 51\%$ ; iv)  $\text{LiAlH}_4, 96\%$ ; v)  $\text{TiF}_2, \text{pyridine, quant.}$ ; vi)  $\text{Ni}(\text{COD})_2, \text{bpy}, 1,5\text{-COD then } \mathbf{7}, 4\%$ .

excellent.  $\text{Ni}^0$ -mediated Yamamoto coupling of triflate **7** gave the target compound **THC** in 4% yield.<sup>[11]</sup> The low yield in the last step is probably because a racemic precursor was used. Generally, the reaction of two compounds with the same chirality dimerize, whereas those with different chirality form oligomers. Although the solubility of the isolated **THC** is low in common organic solvents such as benzene, toluene, dichloromethane, and chloroform, it is moderately soluble in carbon disulfide.

The  $^1\text{H}$  NMR spectrum of **THC** consists of only seven peaks in carbon disulfide/ $[\text{D}_2]$ tetrachloroethane (Figure 2a, black), indicating its highly symmetrical structure. The  $^1\text{H}$  NMR spectrum of **THC** showed almost the same characteristics as those of [5]helicene<sup>[12]</sup> and **T5H**,<sup>[6]</sup> except for  $\text{H}_f$  and  $\text{H}_g$ . **THC** is chiral

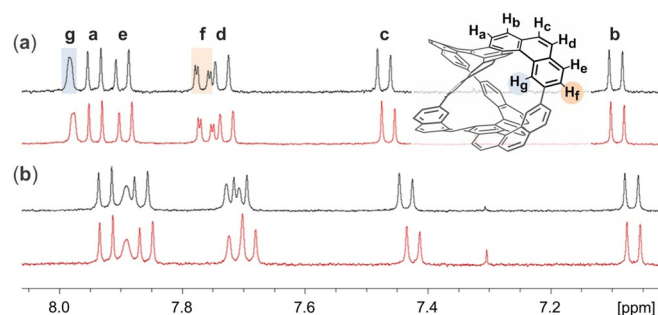


**Figure 2.**  $^1\text{H}$  NMR spectra of **THC** of racemic (black) and the second eluted enantiomer (red) in carbon disulfide/ $[\text{D}_2]$ tetrachloroethane: a) 295 K; b) 233 K.

and each enantiomer was successfully separated by HPLC over a chiral column. The *ee* value of the first and second fractions was 97% (Figure S23).  $^1\text{H}$  NMR spectra of the racemic form and purified second eluted enantiomer of **THC** measured at 295 and 233 K were compared (Figures 2, S21, and S22). Signals assigned to  $\text{H}_f$  and  $\text{H}_g$  showed larger upfield shifts than other signals when the temperature decreased. These two signals are susceptible to environmental change because  $\text{H}_f$  and  $\text{H}_g$  reside at *ortho* positions of the biphenyl moiety, which is the most flexible part of this rigid molecule. Figure 2a shows that the two  $^1\text{H}$  NMR spectra measured at 295 K were almost identical. In contrast, the spectral region at approximately 7.7 ppm showed small differences for these samples measured at 233 K. The spectral differences observed between two stereochemically different samples may reflect differences in the aggregation status between homochiral and heterochiral molecules. This postulate is based on the packing structure of **THC** (Figure 4).

Single crystals for X-ray diffraction analysis were obtained by slow evaporation of carbon disulfide/benzene/toluene solutions of **THC** at room temperature.<sup>[13]</sup> The crystal structure of **THC** revealed that its unit cell contained two crystallographically independent pairs of enantiomers [pairs  $\alpha$  (C1–) and  $\beta$  (C85–)]; space group: *P*-1]. **THC** exhibited a pseudo-threefold rotational axis through the centroid of the central benzene ring of the **T5H** moieties. The rigid PAH skeleton ensures that **THC** retains a highly symmetrical structure of the inner cavity, even in the crystal; otherwise, the hollow cavity is usually in a collapsed state. The most unique structural features of **THC** were the cage-shaped structure with outer helical grooves and the inner chiral cavity (Figures 3a, 3b, and S24). Six [5]helicene moieties in **THC** have the same helicity, all-*P* [(*P*)-**THC**] and all-*M* [(*M*)-**THC**] forms. **THC** in the  $\alpha$  and  $\beta$  pair has 43 and 52 Å<sup>3</sup> of inner void space, respectively. The distances between the two benzene rings located centrally at the top and bottom of the **T5H** moieties are 6.32 Å (for  $\alpha$ ) and 6.33 Å (for  $\beta$ ). Structural analysis revealed that **THC** has a cavity like a three-leaf clover, including a 3.36 Å diameter inscribed sphere. The electron density inside the cage is too low to identify any guests. Even *N,N*-dimethylformamide, the solvent for the synthesis of **THC**, is larger than the cavity size. The windows of **THC** are very narrow and small molecules such as carbon disulfide used in the recrystallization process cannot gain access. The dihedral angles, defined as the angle formed by the two benzene rings located at the terminal edges of each [5]helicene subunit, of the six [5]helicene moieties (average: 57.7° for  $\alpha$  and 58.3° for  $\beta$ , Table S1) are larger than the three [5]helicene moieties of **T5H** (average: 52.8°). Three single bonds between two **T5H** units hoist opposite [5]helicene arms toward each other to make the dihedral angles wider in **THC** (Figure S25).

Distances between two carbon atoms at the tip of the fjord region in the [5]helicene moieties of **THC** were 3.000 Å (average for  $\alpha$ ) and 3.007 Å (average for  $\beta$ ) (Table S2), which are longer than those in **T5H** (average: 2.927 Å). The C–C bond between two benzene rings of biphenyl moieties in **THC** (Table S2) were normal values for biphenyl compounds. To evaluate the local aromaticity of the individual rings, the har-

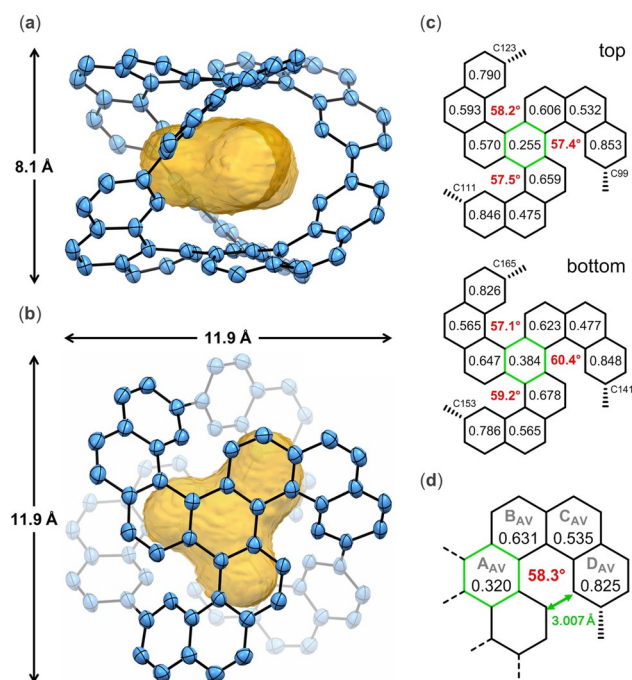


**Figure 3.** X-ray structures of (P)-THC-β: a) side and b) top view. ORTEP drawings are shown at 50% probability. Hydrogen atoms are omitted for clarity. Approximate distances are provided within the double-headed arrows. The solvent accessible void (1.2 Å probe) is depicted in orange. c) Individual and d) averaged HOMA values (black numbers in rings) and dihedral angles (red numbers) are shown.

monic oscillator model of aromaticity<sup>[14]</sup> (HOMA) values were calculated. Central green-colored benzene rings A and K (Figures 3 c and 3 d; for ring naming see Table S1) have the lowest HOMA value (average: 0.402 for  $\alpha$  and 0.320 for  $\beta$ ) in **THC**, which is similar to that in **T5H** (0.302). In contrast, HOMA values of the central benzene ring in **HBTP** (0.711) and **H5H** (0.687) are far higher than that found in **THC**. These differences are derived from symmetric properties where **HBTP** and **H5H** have  $D_3$  symmetry, whereas **T5H** has lower  $C_3$  symmetry that causes more distortion at ring  $A_{AV}$  ( $A_{AV}$  denotes the averaged properties of rings A and K; Table S1) in **THC**. Bond alternation of ring  $A_{AV}$  in **THC** is larger than those in **HBTP** and **H5H** (Table S2). Although the bond lengths at fused positions of ring  $A_{AV}$  in **THC** are comparable with those in **HBTP** and **H5H**, those of non-fused positions in **THC** are longer than those in **HBTP** and **H5H**. The HOMA values for rings  $B_{AV}$  and  $C_{AV}$  are moderate [0.618 and 0.500 (for  $\alpha$ ), 0.631 and 0.535 (for  $\beta$ )] and the HOMA value for ring  $D_{AV}$  is high with values of 0.846 (for  $\alpha$ ) and 0.825 (for  $\beta$ ). These values are almost the same as those in **T5H**, indicating that strains caused by annulation are effectively dispersed across the whole molecule. The crystal structure of **THC** matched well with that of the optimized structure obtained by DFT calculations [B3LYP/6–31-G(d)], indicating that there is little influence residing in the crystal (Table S3). Strain energies of **THC** and **T5H** were calculated to be 79.6 and 38.2 kcal mol<sup>-1</sup>, respectively (DFT at the same level of theory). An increase in the strain energy by 3.2 kcal mol<sup>-1</sup> corresponds to the distortion caused by cage formation (Figure S26). Structural similarity between **T5H** and **THC** implies that our synthe-

tic strategy using a distorted and preorganized precursor to construct a cage compound is effective. Three helical grooves in **THC** of both enantiomers intercalate with each other (Figure 4 a). One (P)-**THC** is surrounded by three (M)-**THCs**, and vice versa, to form a lamellar structure. A void space surrounded by six **THC** molecules, which is filled with solvent molecules (see the Supporting Information) is connected to each other to form a 1D column, thereby forming a crystal honeycomb structure (Figures 4 b and 4 c). Strong  $\pi$ - $\pi$  interactions make this compound barely soluble in various solvents.

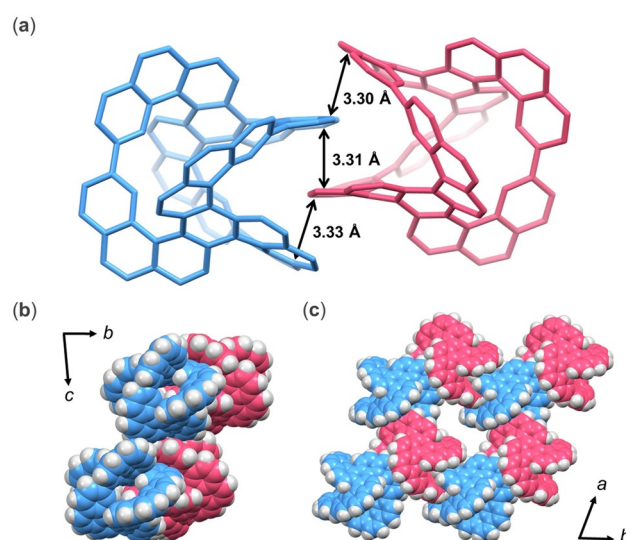


**Figure 4.** Crystal packing of **THC**. (P)-**THC** and (M)-**THC** are shown in blue and pink, respectively. a) The shortest C–C distances between neighboring enantiomers are provided. b) View along the *a* axis. c) View along the *c* axis. Solvent molecules are omitted for clarity.

The photophysical properties of **THC** were measured in chloroform (Figure 5). Determining the precise extinction coefficient by UV/Vis spectral analysis was difficult because of low solubility. The absorption maximum of **THC** was observed at 346 nm, which is 6 nm shorter than that of **T5H**. This small blueshift is presumably caused by a decrease in the effective conjugation. **THC** exhibits weak fluorescence at 470 nm ( $\lambda_{ex}$  = 346 nm) with a low fluorescence quantum yield of 0.017, which is comparable to those of **T5H** ( $\phi$  = 0.026), **H5H** ( $\phi$  = 0.039), and other helicenes.<sup>[15]</sup> In the circular dichroism (CD) spectrum of **THC**, the first peak of the two fractions eluted by chiral HPLC exhibits a positive Cotton effect over the ranges of 366–430 and 285–342 nm, whereas a negative Cotton effect was observed at 342–366 and below 285 nm (Figure 5). The second eluting peak showed a mirror-imaged CD spectrum against the first one. Simulated CD spectra of (P)- and (M)-**THC** prepared by using TDDFT calculations match those observed for the first and second eluted peaks, respectively (Figure S27). The anisotropy factors (*g* values:  $g = \Delta\epsilon/\epsilon$ ) of the first eluting enantiomer of **THC** are  $+13.3 \times 10^{-3}$  (400 nm) and  $+13.9 \times 10^{-3}$  (309 nm). These *g* values are higher than those of **T5H** [(P)-isomer,  $g = +7.8 \times 10^{-3}$  at 281 nm], **H5H** [(P,M,P,M,P,M)-isomer,  $g = -4.8 \times 10^{-3}$  at 324 nm], (P)-(+)-[5]helicene ( $g = +4.2 \times 10^{-3}$

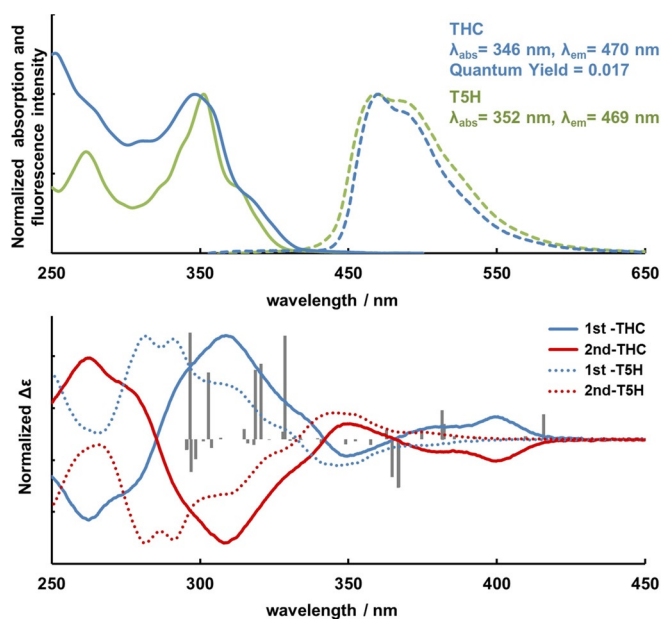


**Figure 5.** Optical properties of **THC** and **T5H** in chloroform. Upper panel: UV/Vis absorption (solid line) and fluorescence spectra (dotted line) of **THC** (blue) and **T5H** (green). Lower panel: CD spectra of **THC** (solid line) and **T5H** (dotted line). The gray bars show the TDDFT-derived rotatory strength values for (P)-**THC** at the B3LYP/6-31G(d) level.

at 310 nm), and (P)-(+)-[6]helicene ( $g = +9.2 \times 10^{-3}$  at 324 nm).<sup>[16]</sup> The high  $g$  values observed for **THC** arise from its characteristic structure with six [5]helicene units that have the same helicity.

The calculated HOMO and LUMO energy levels for **THC** were  $-5.12$  and  $-1.64$  eV, respectively (Figure S28). The former is higher than that for **T5H** ( $-5.29$  eV), and the latter is lower than that obtained for **T5H** ( $-1.60$  eV) at the same level of theory, which means that the HOMO–LUMO energy gap of **THC** (3.48 eV) is reduced when compared with that of **T5H** (3.69 eV).

In summary, the synthesis of **THC**, a 3D cage-shaped molecule composed of six [5]helicene units, is reported. The key to the successful synthesis of **THC** is the use of the rigid and pre-organized **T5H** precursor in the Yamamoto coupling reaction. The structure of **THC** was unambiguously determined by single-crystal X-ray diffraction analysis. **THC** is chiral with unique structural features; outer helical grooves and an inner chiral cavity caused by the six [5]helicene moieties. Our synthetic strategy to construct this cage-shaped molecule provides a new method to synthesize novel 3D  $\pi$ -conjugated molecules. The inherently chiral **THC** should facilitate the study of 3D chiral nanocarbons.

## Acknowledgements

This work was supported by MEXT-Supported Program for the Strategic Research Foundation at Private Universities, 2012–2016

(Grant S1201034). This work was also supported in part by a Faculty of Science Grant-in-Aid for Scientific Research (2017) from Toho University. The computations were performed using the Research Center for Computational Science, Okazaki, Japan.

## Conflict of Interest

The authors declare no conflict of interest.

**Keywords:** aromaticity · chirality · multiple helicene · polycyclic aromatic hydrocarbons ·  $\pi$ -conjugated cages

- [1] a) Y. Segawa, H. Ito, K. Itami, *Nat. Rev. Mater.* **2016**, *1*, 15002; b) Y. Segawa, A. Yagi, K. Matsui, K. Itami, *Angew. Chem. Int. Ed.* **2016**, *55*, 5136–5158; *Angew. Chem.* **2016**, *128*, 5222–5245; c) S. Yamago, E. Kayahara, T. Iwamoto, *Chem. Rec.* **2014**, *14*, 84–100; d) T. Kawase, H. Kurata, *Chem. Rev.* **2006**, *106*, 5250–5273.
- [2] G. Povie, Y. Segawa, T. Nishihara, Y. Miyauchi, K. Itami, *Science* **2017**, *356*, 172–175.
- [3] a) Z. Wu, S. Lee, J. S. Moore, *J. Am. Chem. Soc.* **1992**, *114*, 8730–8732; b) H.-E. Högberg, B. Thulin, O. Wennerström, *Tetrahedron Lett.* **1977**, *18*, 931–934; c) Y. Rubin, T. C. Parker, S. I. Kahn, C. L. Holliman, S. W. McElvany, *J. Am. Chem. Soc.* **1996**, *118*, 5308–5309; d) Y. Rubin, T. C. Parker, S. J. Pastor, S. Jalisatgi, C. Boule, C. L. Wilkins, *Angew. Chem. Int. Ed.* **1998**, *37*, 1226–1229; *Angew. Chem.* **1998**, *110*, 1353–1356; e) Y. Tobe, N. Nakagawa, K. Naemura, T. Wakabayashi, T. Shida, Y. Achiba, *J. Am. Chem. Soc.* **1998**, *120*, 4544–4545; f) Y. Tobe, N. Nakagawa, J. Kishi, M. Sonoda, K. Naemura, T. Wakabayashi, T. Shida, Y. Achiba, *Tetrahedron* **2001**, *57*, 3629–3636; g) Y. Tobe, R. Umeda, M. Sonoda, T. Wakabayashi, *Chem. Eur. J.* **2005**, *11*, 1603–1609.
- [4] a) K. Matsui, Y. Segawa, T. Namikawa, K. Kamada, K. Itami, *Chem. Sci.* **2013**, *4*, 84–88; b) K. Matsui, Y. Segawa, K. Itami, *J. Am. Chem. Soc.* **2014**, *136*, 16452–16458.
- [5] E. Kayahara, T. Iwamoto, H. Takaya, T. Suzuki, M. Fujitsuka, T. Majima, N. Yasuda, N. Matsuyama, S. Seki, S. Yamago, *Nat. Commun.* **2013**, *4*, 2694.
- [6] H. Saito, A. Uchida, S. Watanabe, *J. Org. Chem.* **2017**, *82*, 5663–5668.
- [7] a) L. Barnett, D. M. Ho, K. K. Baldrige, R. A. Pascal, *J. Am. Chem. Soc.* **1999**, *121*, 727–733; b) D. Peña, D. Pérez, E. Guitián, L. Castedo, *Org. Lett.* **1999**, *1*, 1555–1557.
- [8] T. Hosokawa, Y. Takahashi, T. Matsushima, S. Watanabe, S. Kikkawa, I. Azumaya, A. Tsurusaki, K. Kamikawa, *J. Am. Chem. Soc.* **2017**, *139*, 18512–18521.
- [9] a) F. B. Mallory, C. W. Mallory, *Org. React.* **1984**, *30*, 1–456; b) F. B. Mallory, C. S. Wood, J. T. Gordon, *J. Am. Chem. Soc.* **1964**, *86*, 3094–3102; c) C. S. Wood, F. B. Mallory, *J. Org. Chem.* **1964**, *29*, 3373–3377.
- [10] T. Matsushima, S. Kobayashi, S. Watanabe, *J. Org. Chem.* **2016**, *81*, 7799–7806.
- [11] Recent reports describing the use of Yamamoto coupling to construct 3D molecules: a) D. Myśliwiec, M. Kondratowicz, T. Lis, P. J. Chmielewski, M. Stépień, *J. Am. Chem. Soc.* **2015**, *137*, 1643–1649; b) X. Gu, T. Y. Gopalakrishna, H. Phan, Y. Ni, T. S. Herng, J. Ding, J. Wu, *Angew. Chem. Int. Ed. Angew. Chemie Int. Ed.* **2017**, *56*, 15383–15387.
- [12] A. Ayalon, M. Rabinovitz, *Tetrahedron Lett.* **1992**, *33*, 2395–2398.
- [13] CCDC 1813934 contains the supplementary crystallographic data for this paper. These data can be obtained free of charge from The Cambridge Crystallographic Data Centre.
- [14] a) J. Kruszewski, T. M. Krygowski, *Tetrahedron Lett.* **1972**, *13*, 3839–3842; b) T. M. Krygowski, M. K. Cyrański, *Chem. Rev.* **2001**, *101*, 1385–1419.
- [15] M. Sapir, E. V. Donckt, *Chem. Phys. Lett.* **1975**, *36*, 108–110.
- [16] Y. Nakai, T. Mori, Y. Inoue, *J. Phys. Chem. A* **2012**, *116*, 7372–7385.

Received: January 10, 2018

Version of record online February 16, 2018